IOP PUBLISHING NANOTECHNOLOGY
Nanotechnology **18** (2007) 095706 (4pp) doi:10.1088/0957-4484/18/9/095706

Structure and electronic properties of self-assembled Pt silicide nanowires on Si(100)

Do Kyung Lim[1], Dohyun Lee[1,6], Hangil Lee[2], Sung-Soo Bae[1], Junghun Choi[1], Sehun Kim[1], Chengxiang Ji[3], Regina Ragan[4], Douglas A A Ohlberg[5], Y Austin Chang[3] and R Stanley Williams[5]

[1] Department of Chemistry and School of Molecular Science (BK 21), Korea Advanced Institute of Science and Technology, Daejeon 305-701, Republic of Korea
[2] Beamline Research Division, Pohang Accelerator Laboratory (PAL), Pohang University of Science and Technology, Pohang 790-784, Republic of Korea
[3] Department of Materials Science and Engineering, 1509 University Avenue, University of Wisconsin-Madison, WI 53706, USA
[4] Department of Chemical Engineering and Materials Science, University of California, Irvine, CA 92697, USA
[5] Quantum Science Research, Hewlett-Packard Laboratories, 1501 Page Mill Road, MS 1123, Palo Alto, CA 94304, USA

E-mail: sehun-kim@kaist.ac.kr

Received 21 October 2006, in final form 23 November 2006
Published 24 January 2007
Online at stacks.iop.org/Nano/18/095706

Abstract
We investigated the formation of Pt silicide nanowires on a Si(100) surface using scanning tunnelling microscopy and high-resolution photoemission spectroscopy. Pt silicide nanowires with a tetragonal Pt_2Si structure are formed along the step edges of Si(100). Pt-induced $c(4 \times 2)$ reconstructions also appear adjacent to the tetragonal Pt_2Si nanowires. Formation of the Pt_2Si nanowires is attributed to the anisotropic lattice mismatches between the tetragonal Pt_2Si structure and Si(100). Scanning tunnelling spectroscopy data show that the nanowires are metallic. The stoichiometry of Pt silicide is confirmed by high-resolution photoemission spectroscopy.

Low-dimensional structures on the nanometre scale have attracted much interest due to their potential applications in nanoelectronic devices and biosensors. In particular, hexagonal rare-earth disilicide ($RESi_{2-x}$; RE = Sm [1, 2], Dy [1–5, 7], Er [1, 2, 6, 7], or Gd [1, 7–9]) nanowires (NWs) on Si(100) surfaces have been intensively studied by utilizing the anisotropic lattice mismatches between the hexagonal $RESi_{2-x}$ and the Si(100) surfaces. However, the high chemical reactivity of RE metals in the atmospheric environment has made it difficult to work with such materials because they are easily changed into RE metal oxides. On the other hand, the platinum group metals, which are the six heaviest members of Groups 8–10, do not react with air to form an insulating metal oxide layer in normal conditions and hence have potential as conducting materials, which can be used in semiconductor electronic devices. Prompted by these advantageous properties of platinum group metals, we focused on Pt. Pt on Si(100) [10–15] and Ge(100) [16, 17] surfaces has been intensively studied with the aim of forming metallic NWs.

In this paper we report on the formation of Pt silicide NWs with high aspect ratios on a Si(100) surface. We clarify their structure and electronic properties using scanning tunnelling microscopy (STM), scanning tunnelling spectroscopy (STS) and high-resolution photoemission spectroscopy (HRPES).

All experiments were performed in an ultrahigh vacuum (UHV) chamber with a base pressure of 8.0×10^{-11} Torr. The UHV chamber was equipped with an Omicron VT-STM. Clean Si(100) surfaces were prepared by thermal annealing. The n-type Si(100) substrates were annealed to 1200 °C for 10 s with a pressure $<1 \times 10^{-9}$ Torr, cooled down quickly to 950 °C and held for 1 min. Subsequently, the substrates

[6] Present address: Division of Advanced Technology, Korea Research Institute of Standards and Science, Daejeon, 305-600, Korea.

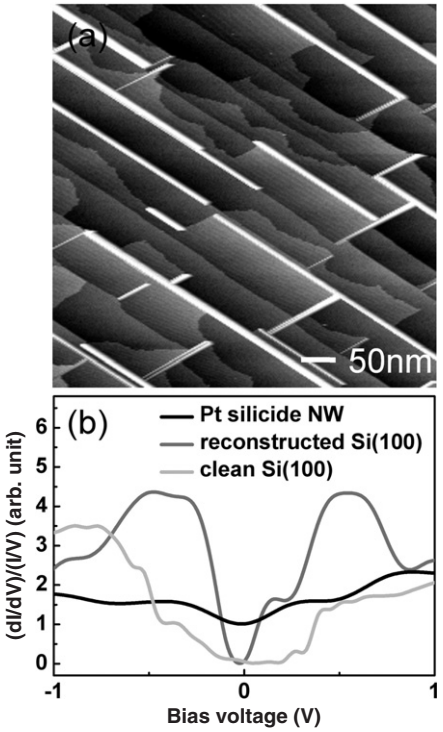

Figure 1. (a) Large-scale STM image showing Pt silicide NWs on Si(100), $V_s = -2.0$ V, $I_t = 0.1$ nA, 550 nm × 550 nm. (b) Normalized STS spectra of a clean Si(100) surface, a reconstructed Si surface and a Pt silicide NW.

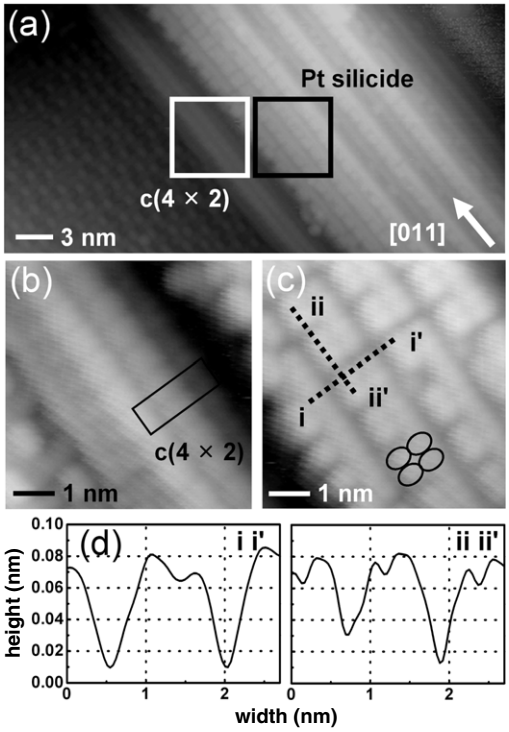

Figure 2. (a) Filled state STM image showing the typical shape of a Pt silicide NW, $V_s = -2.0$ V, $I_t = 0.1$ nA, 40 nm × 20 nm. (b) Filled state image of a $c(4 \times 2)$ reconstructed region. $V_s = -1.0$ V, $I_t = 0.1$ nA, 6 nm × 6 nm. (c) Filled state image of Pt silicide NWs. $V_s = -1.0$ V, $I_t = 0.1$ nA, 6 nm × 6 nm. (d) Line profiles of Pt silicide NWs are shown.

were cooled down slowly at rates of $<2\,^{\circ}$C s^{-1} from 950 °C to room temperature. Native oxide was removed during this high-temperature annealing procedure. The clean Si(100) 2×1 surfaces were confirmed *in situ* using STM. Pt (99.98%) was then deposited on the substrates with an *in situ* e-beam evaporator (OS-Vap, Oxford Scientific) at an emission power of 18 W. During the Pt deposition, the Si(100) surface was maintained at 600 °C below 2.5×10^{-10} Torr. The deposition flux was controlled at 0.05 ML min^{-1} (ML, monolayer). After Pt deposition, the surface was subsequently annealed at 600 °C for 10 min to form a stable Pt silicide with a single phase. STS $I(V)$ curves were obtained with a set point bias of 0.50 V and a set point current of 0.1 nA, then numerically differentiated to derive $\mathrm{d}I/\mathrm{d}V$ curves. The high-resolution core-level photoemission spectra were obtained from a soft x-ray beam-line (8A1) at Pohang Accelerator Laboratory (PAL). Si $2p$ and Pt $4f$ core-level spectra were obtained from a high-performance electron analyser (SES-2002, Gamma Data, Sweden). The measured overall resolutions are 0.25 (0.03) eV with photon energy of 300 (60) eV. All the spectra in our experiments were taken in the normal emission mode and carefully analysed by a standard nonlinear least squares fitting procedure using Voigt functions.

Figure 1(a) shows a large-scale STM image of Pt silicide NWs on a Si(100) surface. After checking a clean Si(100) surface, we deposited 0.25 ML Pt at 600 °C to form the Pt silicide NWs. We have observed self-assembled Pt silicide NWs with a width of a few nanometres and lengths of a few hundred nanometres. The Pt silicide NWs also show unrestricted growth only along the [0 1 1] direction. This asymmetric and orientation dependent growth of Pt silicide NWs suggests the formation of NWs through anisotropic lattice mismatches between Pt silicide crystal and Si(100). At the same time, these NWs can be distinguished from the previously reported three-dimensional (3D) PtSi islands [18] since the size and shape of the PtSi islands have little uniformity. Detailed discussions about the structure of NWs will be made with atomic-resolution STM images in figure 2.

The electronic properties of the NWs fabricated in the present work were determined by STS. The differential conductance $\mathrm{d}I/\mathrm{d}V$, which is proportional to the density of states (DOS) of the sample, is normalized to remove the influence of tip–sample separation and applied bias voltage. Figure 1(b) shows the normalized STS spectra of the Pt silicide NWs and the reconstructed Si(100) surface. The STS spectrum of the clean Si(100) surface is also shown for comparison. The STS spectrum obtained from the Pt silicide NW region shows a higher DOS at E_F than that of the clean Si(100) surface, indicating that the surface with NWs has metallic properties.

To clarify the atomic structure of Pt silicide NWs, we magnified the image of figure 1(a). As shown in figure 2(a), we can clearly see the Pt silicide NW surrounded by line shaped surface reconstructions. The Pt silicide NW consists of single NWs having a width of 1.2 nm each.

Figure 2(b) shows a high-resolution STM image for the reconstructed surface around the Pt silicide NW marked with a white rectangle in figure 2(a). Previously, Ji *et al* reported Pt-induced $c(4 \times 6)$ and $c(4 \times 2)$ reconstructions on the

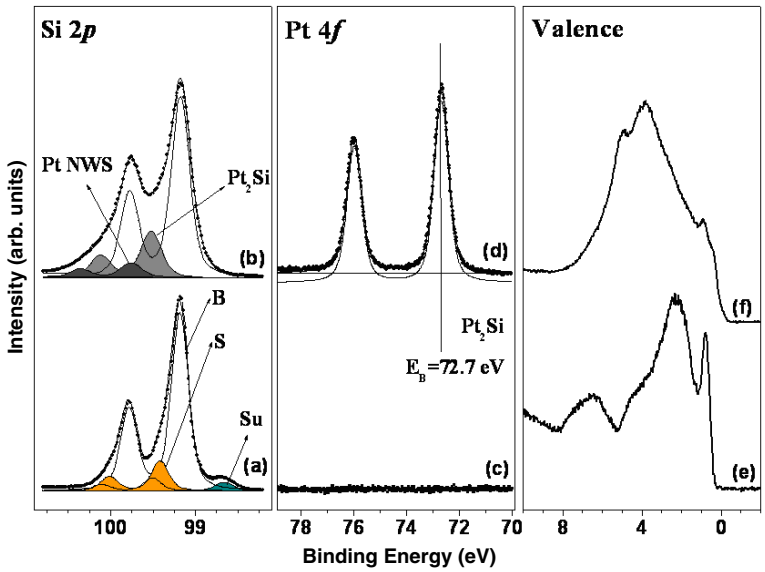

Figure 3. HRPES spectra of clean Si(100) surface for (a) Si 2p, (c) Pt 4f and (e) valence band were compared with the HRPES spectra of Pt silicide NWs for (b) Si 2p, (d) Pt 4f and (f) valence band.
(This figure is in colour only in the electronic version)

terraces of Si(100) [14]. On our STM image in figure 2(b), the $c(4 \times 2)$ reconstructions are obvious and they are assembled successively along a Pt silicide NW taking the shape of satellite lines of the Pt silicide NW. The bright protrusions that constitute the lines on the STM image are Si dimers surrounding a Pt atom. These lines of $c(4 \times 2)$ reconstruction predominantly grow near a Pt silicide NW or at a step edge, indicating that the step edges and Pt silicide NWs act as diffusion barriers, causing Pt atoms diffusing on the terraces to accumulate at these barriers and assemble into satellite lines.

Figure 2(c) shows a typical atomic-resolution STM image of a Pt silicide NW from the area marked with a black rectangle in figure 2(a). In this image, bright oval-shaped protrusions assembled periodically on the top surface of the Pt silicide NWs. The lattice spacings along the [0 1 1] and [0 $\bar{1}$ 1] directions (parallel and perpendicular to the growth direction of the NW) was measured as shown in figure 2(d). The distances between the protrusions in the [0 1 1] and [0 $\bar{1}$ 1] directions were 0.384 and 0.566 nm, respectively. As stated above, these lattice spacings as well as the overall shape of the NWs cannot be explained if the NWs are composed of PtSi. PtSi has the smallest lattice mismatch along the c-axis with the Si(100) substrate, which is as large as 6.7% ($a = 0.591$ nm, $b = 0.557$ nm, $c = 0.358$ nm) [19]. Consequently, PtSi forms 3D islands with irregular sizes and shapes. However, the lattice constants of tetragonal Pt_2Si ($a = 0.394$ nm, $c = 0.596$ nm) [20] agree with the results of the atomic spacing observed on the NW along [0 1 1] and [0 $\bar{1}$ 1] directions. The lattice mismatch between the a-axis of tetragonal Pt_2Si and the Si(100) surface (a_0; 0.384 nm) is only 2.6%, whereas that between the c-axis of tetragonal Pt_2Si and the Si(100) surface is as large as 55.2%. This anisotropic lattice mismatch favours growth of the tetragonal Pt_2Si crystal along the [0 1 1] direction of the Si(100) surface, leading to the formation of Pt_2Si NWs with a high aspect ratio. Moreover, at the perpendicular axis (c-axis $\parallel$ [0 $\bar{1}$ 1]), double the lattice constant of tetragonal Pt_2Si is roughly equal to three times that of the Si(100) surface (2×0.596 nm $\approx 3 \times 0.384$ nm with a lattice mismatch of 3.5%). Therefore, to minimize strain during the formation of the Pt_2Si NW, the width of the single NW along the [0 $\bar{1}$ 1] direction mainly corresponds to two unit cell lengths of the tetragonal Pt_2Si crystal, as shown in figure 2(c).

Although we estimated that the NWs consisted of Pt_2Si crystal in accordance with the line profile data, it was still controversial whether they were PtSi or Pt_2Si. Hence, we performed HRPES to confirm the stoichiometry of Pt silicide NWs directly from HRPES analysis. Figure 3(a) shows a clean Si 2p core-level spectrum, which is resolved into three well-defined peaks. Each peak depicts the bulk (marked as B), the second Si layer (marked as S) and the upper dimer surface (marked as S_u) with binding energies of 99.2 eV (bulk), 99.4 eV (S), and 98.6 eV (S_u), which are well matched to the previous results [21, 22]. After checking Pt silicide NWs with $c(4 \times 6)$ surface reconstruction using LEED (not shown here), we obtained the Si 2p core-level spectrum as shown in figure 3(b).

In this spectrum, we observed two remarkable changes, compared to the clean Si 2p spectrum. First, the deposition of Pt leads to the disappearance of the peaks S_u and S of the clean Si surface. This may possibly be caused by the redistribution of electron density and the Pt silicide-induced $c(4 \times 6)$ reconstruction. Secondly, two new peaks with large intensity, which we regard as Pt silicide-induced peaks, start to appear. These two peaks are located at a binding energy region 0.35 and 0.44 eV higher, respectively, than the bulk Si 2p core-level spectrum. Here, we can assign the peak which shows a relatively low chemical shift as Pt silicide at the subsurface of Si and the other peak as Pt silicide NW.

Based on Pt 4f core-level and valence band spectra of Pt silicide NWs in figures 3(d) and (f), we may determine the stoichiometry of NWs. In figure 3(d), the Pt 4f core-level spectrum of Pt silicide NW has a binding energy at 72.7 eV

(the binding energy of PtSi is 73.0 eV) which is well matched to the previously reported binding energy of Pt_2Si. The overall shape of the valence spectrum, which is shown in figure 3(f), also agrees with the Pt *d*-band shift of Pt_2Si [23]. As a result, we can exclude the possibility that Pt silicide NWs could have the stoichiometry of PtSi.

It has been reported previously that the Pt thickness and annealing temperature affect the phase of Pt silicide formed on Si(100) [24]. Under different deposition conditions, Kavanagh *et al* [18] observed the formation of PtSi islands on Si(100) after deposition of Pt on the Si substrate at relatively high temperatures (over 750 °C) and high coverage ($4.8 \pm 0.1 \times 10^{15}$ cm^{-2} $\approx$ 9.34 ML). However, as shown in the HRPES spectra in figure 3, we could effectively suppress the growth of PtSi and induce Pt_2Si formation by controlling the annealing temperature and thickness. At such low Pt coverage as in our experimental conditions it is difficult for PtSi to grow directly because of the large lattice mismatch between the PtSi crystal and the Si(100) surface. These results are also compatible with the phase diagram of the Pt–Si system, according to which Pt_2Si undergoes a polymorphic transition at 695 °C from a tetragonal structure (tI6) to a hexagonal structure (hP6), and PtSi is stable up to 975 °C [19].

In summary, we have investigated the formation of Pt silicide NWs on a Si(100) surface using STM and HRPES. The STM images showed that Pt silicide NWs are formed with a high aspect ratio unrestricted along the step edges of a Si(100) surface. The NWs consist of satellite lines of $c(4 \times 2)$ reconstructions and tetragonal Pt_2Si NWs. The $c(4 \times 2)$ reconstructions are formed at step edges and adjacent to the tetragonal Pt_2Si NWs, which act as barriers to thermal diffusion of adsorbed Pt atoms on the substrate. The tetragonal Pt_2Si NWs are ascribed to anisotropic lattice mismatches between the tetragonal Pt_2Si structure and the Si(100) surface, similar to the case of hexagonal $RESi_{2-x}$ NWs. A single tetragonal Pt_2Si NW has a lateral width as narrow as 1.2 nm, which corresponds to two unit cells of the tetragonal Pt_2Si crystal. For the properties of the Pt silicide NWs, we confirmed that they have a tetragonal Pt_2Si structure and also that their electronic structures are metallic by HRPES and STS analysis. Given the stability of Pt against oxidation, as well as its high (n-type) and low (p-type) Schottky barrier at the interface with Si, Pt_2Si NWs are likely to find applications in the fabrication of nanoelectronic devices.

Acknowledgments

This work was supported by the Brain Korea 21 project, the SRC programme (Center for Nanotubes and Nanostructured Composites) of MOST/KOSEF, and the National R&D Project for Nano Science and Technology. It was also partly supported by grant no. R01-2006-000-11247-0 from the Basic Research Program of the Korea Science and Engineering Foundation, grant no. KRF-2005-070-C00063 from the Korea Research Foundation, and grant no. NSF-DMR-0097621 from US National Science Foundation.

References

[1] Lee D, Lim D K, Bae S-S, Kim S, Ragan R, Ohlberg D A A, Chen Y and Williams R S 2005 *Appl. Phys.* A **80** 1311
[2] Ragan R, Chen Y, Ohlberg D A A, Medeiros-Ribeiro G and Williams R S 2003 *J. Cryst. Growth* **251** 657
[3] Preinesberger C, Pruskil G, Becker S K, Dähne M, Vyalikh D V, Molodtsov S L, Laubschat C and Schiller F 2005 *Appl. Phys. Lett.* **87** 083107
[4] Preinesberger C, Vandrė S, Kalka T and Dähne P 1998 *J. Phys. D: Appl. Phys.* **31** L43
[5] Nogami J, Liu B Z, Katkov M V, Ohbuchi C and Birge N O 2001 *Phys. Rev.* B **63** 233305
[6] Chen Y, Ohlberg D A A, Medeiros-Ribeiro G, Chang Y A and Williams R S 2000 *Appl. Phys. Lett.* **76** 4004
[7] Chen Y, Ohlberg D A A and Williams R S 2002 *J. Appl. Phys.* **91** 3213
[8] Lee D and Kim S 2003 *Appl. Phys. Lett.* **82** 2619
[9] McChesney J L, Kirakosian A, Bennewitz R, Crain J N, Lin J-L and Himpsel F J 2002 *Nanotechnology* **13** 545
[10] Nelson A J, Danailov M, Barinov A, Kaulich B, Gregoratti L and Kiskinova M 2002 *Appl. Phys. Lett.* **81** 3981
[11] Li M C, Chen X, Cai W, Yin J, Yang J, Wu G and Zhao L 2001 *Mater. Chem. Phys.* **72** 85
[12] Dharmadhikari C V, Ali A O, Suresh N, Phase D M, Chaudhari S M, Ganesan V, Gupta A and Dasannacharya B A 2000 *Solid State Commun.* **114** 377
[13] Nishikawa K, Yamamoto M, Ichimiya K, Umetani Y and Kingetsu T 1995 *Japan. J. Appl. Phys.* **34** 3336
[14] Ji C, Ragan R, Kim S, Chang Y A, Chen Y, Ohlberg D A A and Williams R S 2005 *Appl. Phys.* A **80** 1301
[15] Ragan R, Kim S, Li X and Williams R S 2005 *Appl. Phys.* A **80** 1339
[16] Gurlu O, Zandvliet H J W, Poelsema B, Dag S and Ciraci S 2004 *Phys. Rev.* B **70** 085312
[17] Gurlu O, Adam O A O, Zandvliet H J W and Polesema B 2003 *Appl. Phys. Lett.* **83** 4610
[18] Kavanagh K L, Reuter M C and Tromp R M 1997 *J. Cryst. Growth* **173** 393
[19] Massalski T B (ed) 1990 *Binary Alloy Phase Diagrams* 2nd edn, vol 3 (USA: Alloy Phase Diagram International Commission)
[20] Pearson W B *et al* (ed) 1996 *Pearson's Handbook of Crystallographic Data for Intermetallic Phases* 2nd edn, vol 4 (Metals Park, OH: American Society for Metals)
[21] Koh H, Kim J W, Choi W H and Yeom H W 2003 *Phys. Rev.* B **67** 07306
[22] Kim Y K, Lee M H and Yeom H W 2005 *Phys. Rev.* B **71** 115311
[23] Grunthaner P J, Grunthaner F J and Madhukar A 1982 *J. Vac. Sci. Technol.* **20** 680
[24] Das S R, Sheergar K, Xu D-X and Naem A 1994 *Thin Solid Films* **253** 467